Circulation Patterns Near the Tail of the Grand Banks[1]

G. M. VOORHEIS,[2] K. AAGAARD AND L. K. COACHMAN

Dept. of Oceanography, University of Washington, Seattle 98195

(Manuscript received 26 February 1973, in revised form 4 June 1973)

ABSTRACT

Dynamic topographies for the region surrounding the tail of the Grand Banks have been examined for the years 1922–65, in an attempt to define the characteristics of the eddies and meanders typical of the circulation pattern. The size distribution of the cyclonic eddies appears to be bimodal and thus suggests the possibility of two different modes of eddy formation. The shear of the mean current system is cyclonic, and it is therefore not surprising that cyclonic eddies dominate over anticyclonic ones by 2.5:1. However, the anticyclonic eddies appear faster; this may in part be associated with the choice of reference level. Other than a seasonal decrease in eddy strength from April–June, no secular trends could be found. The eddies were characteristically found in certain areas only, suggesting that topography plays a role in their formation. The meanders were markedly smaller and slower than those of the Kuroshio front. No secular trends could be found in the meander patterns. A simple vorticity analysis indicates the meander pattern to be bathymetrically controlled.

1. Introduction

The region near the tail of the Grand Banks has long been of particular oceanographic interest. The need for iceberg drift prediction precipitated by the *Titanic* disaster in 1912 provided the initial stimulus for systematic study. However, the area is of interest in a more general way because it is the confluence zone of the Atlantic and Labrador currents and also the region in which the Atlantic Current leaves the continental margin.

The circulation is dominated by the Labrador Current carrying cold (0–4C) low-salinity (33–34.9‰) water southward along the eastern edge of the Grand Banks and by the counterflowing Atlantic Current carrying warm (4–14C) saline (35.0–35.8‰) water farther offshore. Between the two flows, a region of mixed water of intermediate characteristics forms a trough in the dynamic topography. In addition, there is usually a pattern of meanders and eddies indicated by the topography.

The oceanographic data are distinguished by a series of hydrographic observations, largely conducted on an annual basis by the International Ice Patrol (IIP), which are unique in terms of accuracy and time span. The remarkable quality of the data is in large part due to the dedication of Floyd Soule, who conducted these surveys from 1933–63. We have examined the data with a view toward determining the persistence and characteristics of the meanders and eddy patterns in the circulation.

[1] Contribution No. 732, Department of Oceanography, University of Washington.

[2] Presently on active duty with the U. S. Navy.

2. Methods

The Ice Patrol cruises during the iceberg season (April–June) were initiated systematically in 1922 and have been conducted annually since then, with the exception of a few years, mostly during World War 2. Eight standard sections have been occupied (R–X in Fig. 1), although it has not been possible to do all sections each year. In 1966, the number of standard sections was reduced to three (2–4 in Fig. 1). Unfortunately, this basic cruise modification reduced the areal coverage such that detailed charts of dynamic topography cannot be constructed with unambiguous definition of wave patterns and eddies, even though these features are obviously present. The length of the cruises has varied from approximately ten days to one month. A list of the cruises examined is given in Appendix A; the possibility of conclusions being biased by the distribution of data is discussed in Appendix B.

Mean dynamic topographies during each month of the iceberg season have been calculated by Soule (unpublished) from 22 years of data and reported by Morgan (1969). They are shown in Figs. 2–4; the meanders are particularly conspicuous. Examination of the dynamic topographies from individual cruises reveals that both eddies and meanders can be defined. We recognize that subjectivity is involved in the description of such features, but considerable effort was made to be internally consistent, and we adopted the following guidelines.

a. Eddies

Only closed contours were interpreted as eddies. For each eddy, a mean diameter and a mean dynamic height gradient were assigned. The selection process is

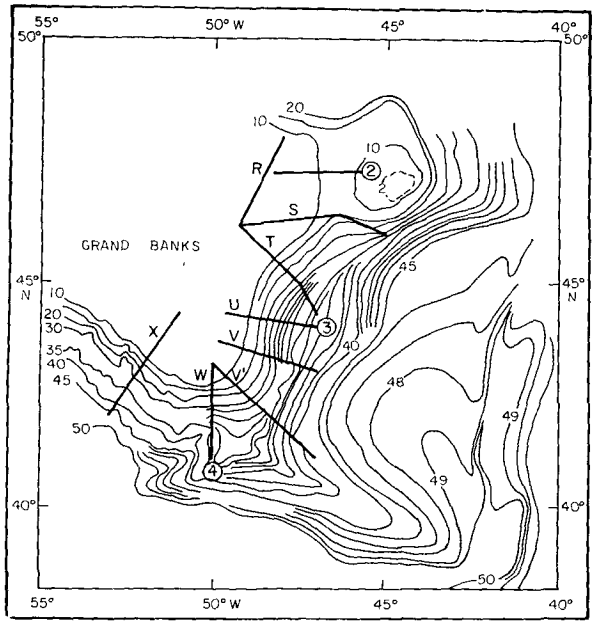

FIG. 1. Bathymetry near the tail of the Grand Banks with depths in hundreds of meters. Sections R–X are the standard International Ice Patrol hydrographic sections. Sections 2–4 are the revised sections begun in 1966.

illustrated in Fig. 5. In addition, the direction of rotation, the location (according to the numbered grid, Fig. 6), and the date were noted. We then calculated the geostrophic speed V_g and the vortex strength $K = \pi \times \text{diameter} \times V_g$. The results for 31 cases are summarized in Table 1 and Figs. 7, 10 and 11. For comparison, the mean speeds calculated from the mean topographies of Soule (Morgan, 1969) are given in Table 2.

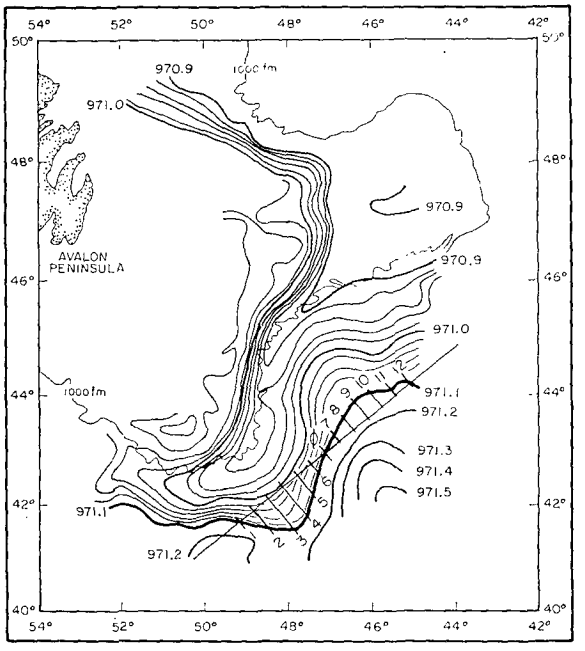

FIG. 2. Mean dynamic topography in dynamic meters for April [after Soule (reported in Morgan, 1969)]. The numbered sections refer to the vorticity computations of Fig. 16.

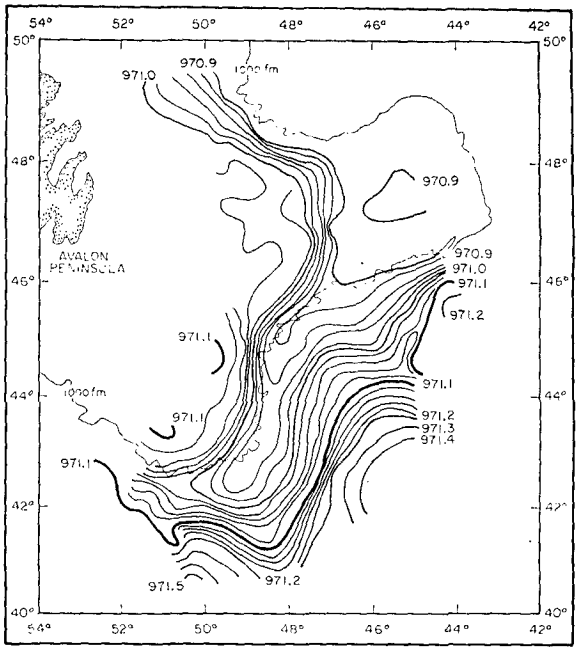

FIG. 3. As in Fig. 2 except for May.

b. *Meanders*

The dynamic height contour 971.1 dynamic meters (hereafter abbreviated dm) was chosen to represent the meander, and the wavelength λ and amplitude A were selected as in Fig. 5. The mean geostrophic speed was

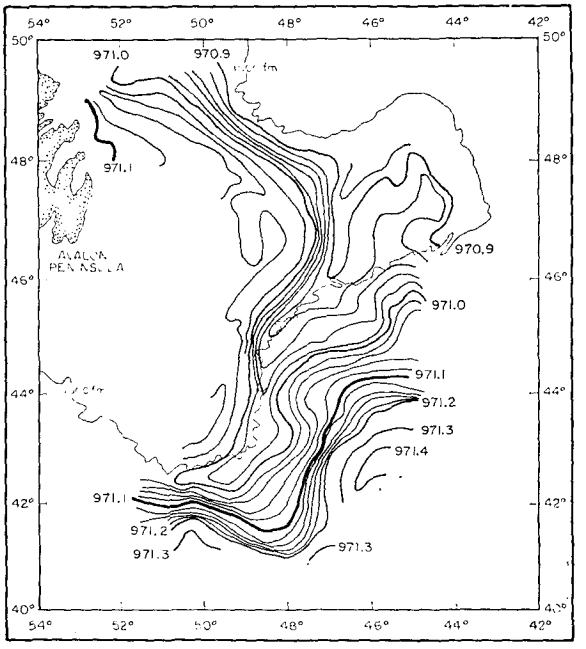

FIG. 4. As in Fig. 2 except for June.

estimated from the mean dynamic height gradient over the wavelength.

The results for 58 cases are summarized in Table 3 and Figs. 12–13.

3. Discussion

a. Eddy characteristics

The monthly mean diameter of the eddies (Table 1a) ranges[3] from 80 to 120 km, with individual cases seldom less than 60 km or more than 140 km. In general, the mean diameters appear to be quite similar for all months; the slight decrease in mean value during May is probably not significant. It is possible that the anticyclonic eddies are somewhat larger than the cyclonic.

The frequency distribution of the diameters (Fig. 7b) indicates that the anticyclonic eddies are skewed toward larger sizes, and although the cyclonic eddies seem more uniformly distributed, there may be a separate class of smaller cyclonic eddies. If so, it suggests the possibility of different modes of cyclonic eddy formation.

The sense of rotation is predominantly cyclonic by a ratio of 2.5:1 (Fig. 7b). Such predominance would be expected if the cyclonic shear of the mean current system is in part responsible for eddy formation.

The anticyclonic eddies appear to be faster (33.4 cm sec^{-1}) than the cyclonic (24.7 cm sec^{-1}), and the somewhat greater mean size and speed of the anticyclonic eddies is such as to give them a significantly larger vortex strength (Table 1a). However, if eddies of both senses of rotation are derived from mean flows of equal strength, then from force balance considerations one would expect them to be about equal; thus,

[3] The value of 75 km for the anticyclonic diameter in June represents a single instance.

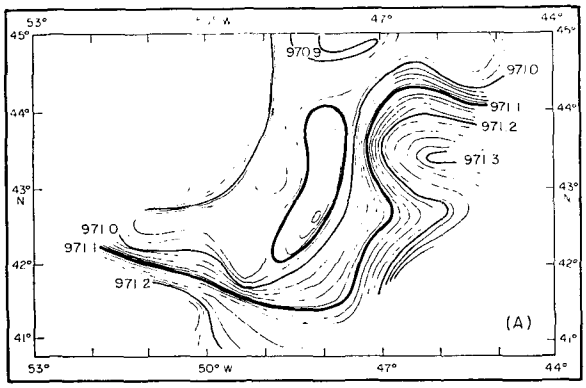

FIG. 5. Dynamic topography, illustrating process of selecting eddy and meander parameters.

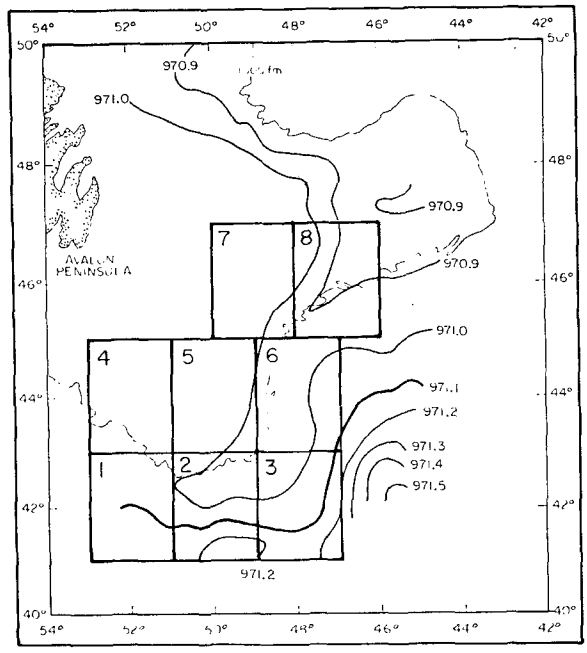

FIG. 6. The grid system used for locating eddies, superimposed on the mean April topography.

TABLE 1. Eddy characteristics.

a. Average diameter and strength.

	Diameter (km)			
	Cyclonic	Anti-cyclonic	All	Strength (cm sec^{-1}×10^8)
April	103	105	104	9.85
May	80	121	95	7.49
June	109	75*	105	8.70
All	100	109	102	8.90
Strength (cm sec^{-1}×10^8)	7.86	11.6	8.90	

b. Average dynamic height gradient and geostrophic speed V_g.

	Dynamic height gradient (dm km^{-1}×10^3)			(V_g)
	Cyclonic	Anticyclonic	All	(cm sec^{-1})
April	2.64	3.42	2.95	29.8
May	2.20	2.75	2.45	24.7
June	2.38	5.00	2.56	25.9
All	2.44	3.30	2.72	27.5
V_g (cm sec^{-1})	24.7	33.4	27.5	

* Based on one observation only.

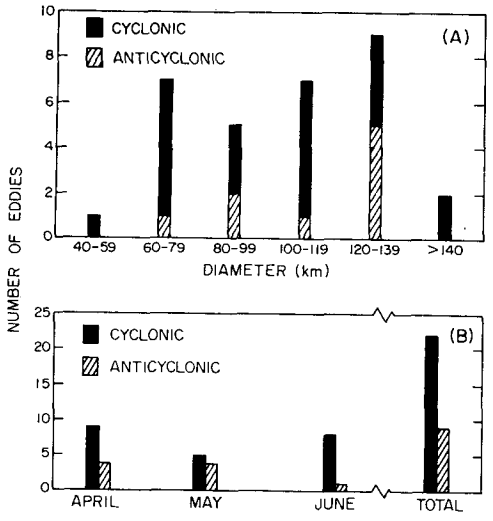

FIG. 7. Distribution of eddy diameters (a) and eddy rotation sense (b).

at latitude 43N, for an eddy radius of 50 km and $V_g = 25$ cm sec^{-1}, the centrifugal acceleration is 1.2×10^{-4} cm sec^{-2}, while the Coriolis acceleration is 2.5×10^{-3} cm sec^{-2}. In the steady state, therefore, the eddies are essentially geostrophic.

It is possible that the greater strength of the anticyclonic eddies may be an artifact of the arbitrary 1000 m reference level chosen for the dynamic topographies, i.e., that the cold-core cyclonic eddies may extend well below this reference level, but that the warm-core anticyclonic eddies have little baroclinicity below 1000 m. The data do not permit significant testing of the hypothesis (the hydrographic sections do not bisect enough eddies, and the observations do not extend below 1000 m), but a possible case in point is illustrated in Figs. 8 and 9. The slope of the sigma-t surfaces is considerably greater at 1000 m in the cyclonic case, so that the strengths of both types of eddies may be more nearly equal than suggested by Table 1a. On the other hand, it is possible that the anticyclonic eddies are derived from a faster parent flow, although Table 2 suggests the contrary.

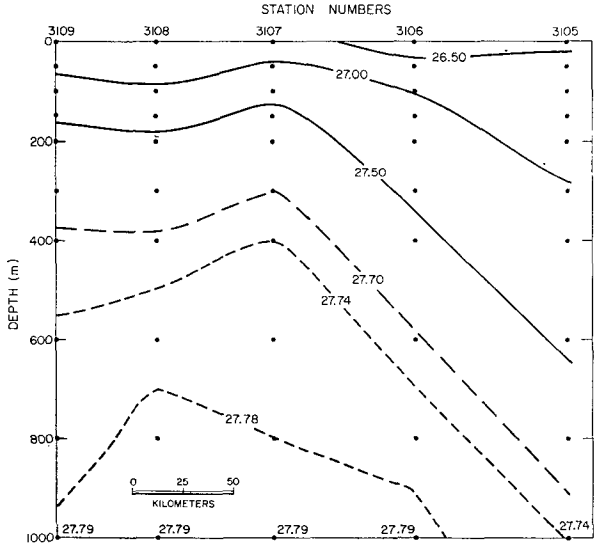

FIG. 8. Sigma-t section across a cyclonic eddy, April 1940.

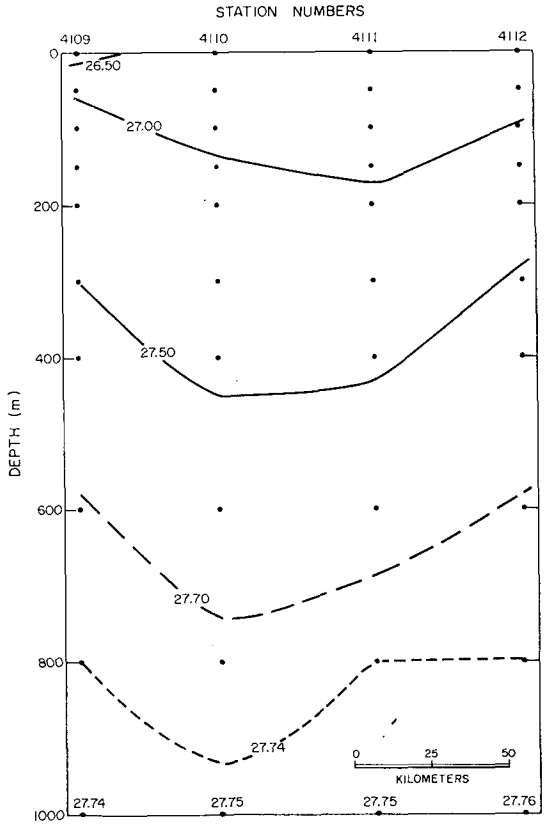

FIG. 9. Sigma-t section across an anticyclonic eddy, May 1950.

The overall mean vortex strength is 8.9×10^{8} cm^2 sec^{-1}. Barkley (1968) found the strength of vortices along the Kuroshio-Oyasio front east of Japan to be $4\text{–}5\times10^{9}$ cm^2 sec^{-1}, i.e., one-half order of magnitude larger. This is because the typical surface geostrophic velocities in the Kuroshio eddies are greater by a factor of perhaps 4, and they are also larger by about one-fourth.

b. Secular trends

No long-term trends in the number, speed or size of eddies could be found (Fig. 10). However, there are

TABLE 2. Mean geostrophic speeds (cm sec^{-1}).

	Section W		Section V	
	Atlantic current	Labrador current	Atlantic current	Labrador current
April	37.0	27.0	20.0	25.0
May	33.8	25.3	16.8	20.6
June	32.0	19.0	18.0	20.0
All	34.3	23.4	18.3	21.5

some indications of seasonal variation. The mean Atlantic and Labrador currents speeds (Table 2) show a definite decrease from April to June. The vortex strength has a minimum in May, but the overall trend is a decrease from April to June (Table 1a). In addition, the frequency of occurrence of eddies shows a definite decrease from 13 eddies in April to 9 each in May and June (Fig. 7b). The overall decrease in eddy strength and number thus coincides with the decrease in strength of the countercurrent system.

c. *Eddy location and formation*

While cyclonic eddies were found to exist throughout most of the area surveyed (Fig. 11), over one-third of them were located in grid space 6, as were all anticyclonic eddies. At a minimum, this suggests that bottom topography plays a role in the formation of the latter. In addition, the anticyclonic eddies were always found in approximately the same position relative to the meander pattern (cf. Fig. 12).

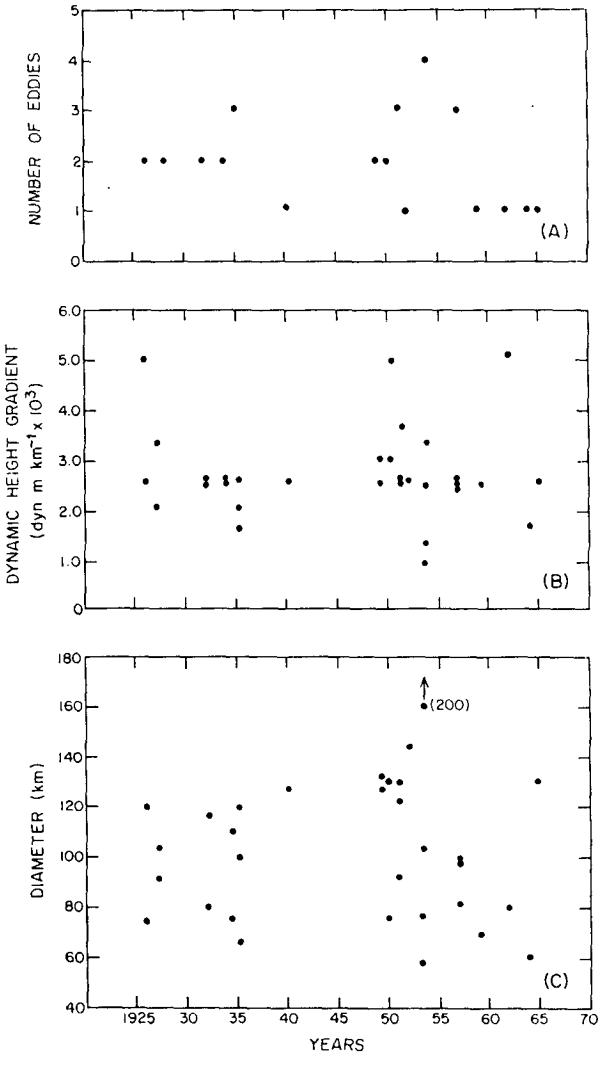

FIG. 10. Yearly distribution of eddy parameters.

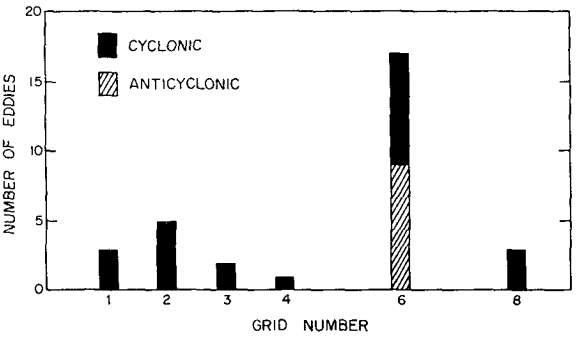

FIG. 11. Location of eddies (see Fig. 6 for grid location).

Figs. 12 and 13 illustrate how the meanders might serve as sources for both cyclonic and anticyclonic eddies. As a crest or trough deepens, it starts to close, and a detached eddy is born. The life span of eddies appears to vary from about one month [an anticyclonic eddy which had formed between April and May 1950 (Fig. 12) appeared to be gone by June, and a new eddy subsequently formed] to a few months [an eddy which formed between April and May 1934 (Fig. 13) still existed in June].

d. *Meander characteristics*

Two types of meander patterns were examined, those with eddies and those without. No significant differences of wavelength, amplitude or current speed were found between the two types (Table 3a).

The wavelengths were distributed rather uniformly between less than 175 km and more than 375 km (Fig. 14a), with a mean of 277 km. Two-thirds of the amplitudes were between 50–100 km, and the overall mean was 78 km. There may be a bimodality in the amplitude distribution (Fig. 14b), possibly related to

TABLE 3. Meander characteristics.

a. As related to eddies.

	Number	Wavelength λ (km)	Amplitude A (km)	$\bar{V}_g$ (cm sec^{-1})
Meanders with no eddies	31	284	75	34.3
Meanders with eddies	27	268	82	33.2
All	58	277	78	33.8

b. Monthly summaries.

	Number	Wavelength λ (km)	Amplitude A (km)	$\bar{V}_g$ (cm sec^{-1})
April	23	278	79	32.4
May	21	274	71	35.0
June	14	283	87	34.1
All	58	277	78	33.8

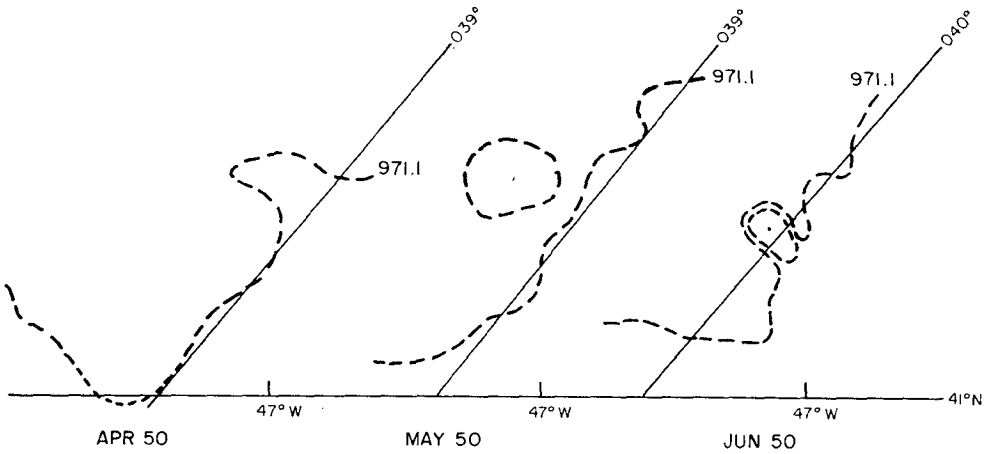

FIG. 12. Formation of two anticyclonic eddies, with contour values in dynamic meters. The meander axis is indicated.

the suggested bimodality in eddy size. In any case, the meanders are markedly smaller, both in length and amplitude, than those east of Japan documented by Barkley (1968). The parameters are compared in Table 4.

Hansen (1970), using the 15C isotherm at 200 m as an indicator of the thermal front of the Gulf Stream east of Cape Hatteras, has found quasi-geostrophic wave patterns with 200–400 km wavelength moving eastward with speeds of 5–10 cm sec^{-1}. While no progression of the wave pattern was found near the Grand Banks (as was also the case in Barkley's investigation) the wavelengths are in close agreement with those of Hansen.

Eighty percent of the surface meander speeds (Fig. 12c) are between 25–40 cm sec^{-1}, with a mean of 33.8 cm sec^{-1}.

e. Secular trends

No significant differences in the meander patterns were found between April, May and June (Table 3b). The similarity between the mean monthly patterns (Figs. 2–4) supports this conclusion. Likewise, no discernible long-term trend was found (Fig. 15).

f. Meander location and formation

Warren (1963) has attempted to describe the meanders of the Gulf Stream as bathymetrically controlled, using vorticity conservation arguments. The applicability of such an argument to the meander patterns in the Grand Banks region was tested in a simple way as follows. Vorticity was calculated in two different ways from the mean April, May and June dynamic topographies (Figs. 2–4). The results were similar for

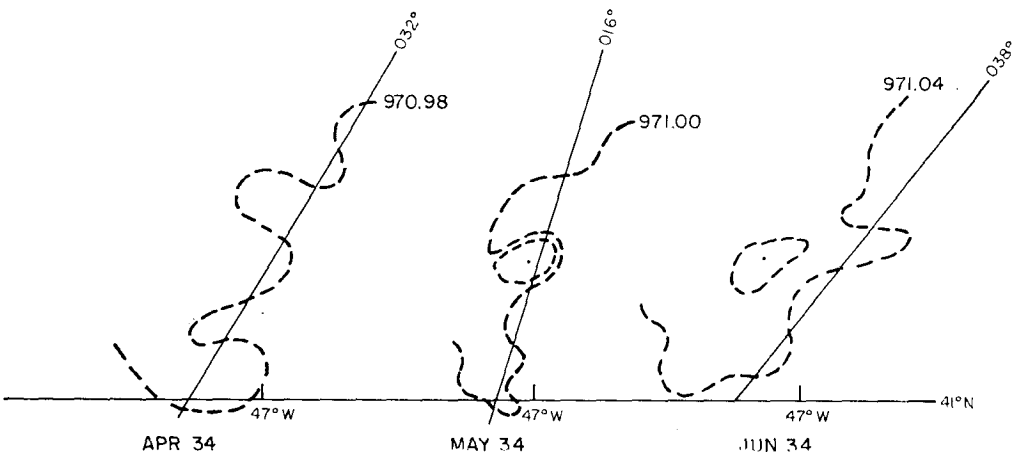

FIG. 13. Formation of a cyclonic eddy, with contour values in dynamic meters. The meander axis is indicated.

each month, so that only those for April are presented here:

1) If we assume for the moment that the flow is geostrophic and barotropic, then the vertical vorticity equation is

$$\frac{\zeta+f}{H}=C,$$

a constant, along a streamline, where $\zeta=(\partial v/\partial x)-(\partial u/\partial y)$ is the relative vorticity, f the Coriolis parameter, and H the water depth. Assume also that the streamlines coincide with the dynamic contours, so that at the wave node $\zeta=0$ (station ϕ in Fig. 2) and C can be evaluated directly. If the depth is known, the relative vorticity can then be calculated at any point along the streamline from the potential vorticity equation, subject to the assumptions of the latter. The parameter CH varies between 0.84×10^{-4} and 1.15×10^{-4} sec^{-1} over the meander, whereas f varies between 0.97×10^{-4} and 1.02×10^{-4} sec^{-1}. In terms of vorticity changes, the stretching effect therefore exceeds the planetary effect by one-half order of magnitude for barotropic flow.

2) In terms of a streamfunction ψ for the real surface flow, defined by $u=-\partial\psi/\partial y$, $v=\partial\psi/\partial x$, we have

$$\zeta=\frac{\partial v}{\partial x}-\frac{\partial u}{\partial y}=\frac{\partial^2\psi}{\partial x^2}+\frac{\partial^2\psi}{\partial y^2}.$$

The streamfunction is thus equivalent to the dynamic height multiplied by $10f^{-1}$. The method of Proudman (1953, p. 115) was used to estimate the second derivatives.

TABLE 4. Comparison of meander parameters.

		Range	Mean
Wavelength λ (km)	Tail of the Banks	<175~>375	277
	Kuroshio-Oyashio	350–460	404
Amplitude A (km)	Tail of the Banks	<40–200	78
	Kuroshio-Oyashio	120–230	170

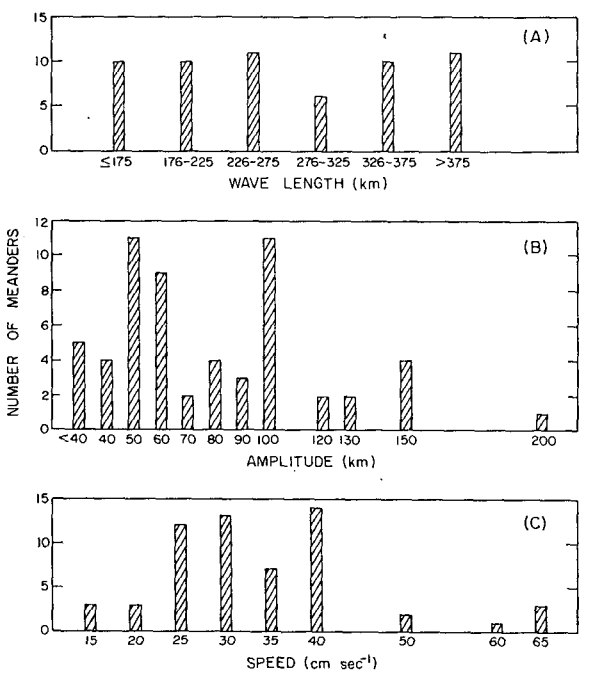

FIG. 14. Distribution of meander parameters.

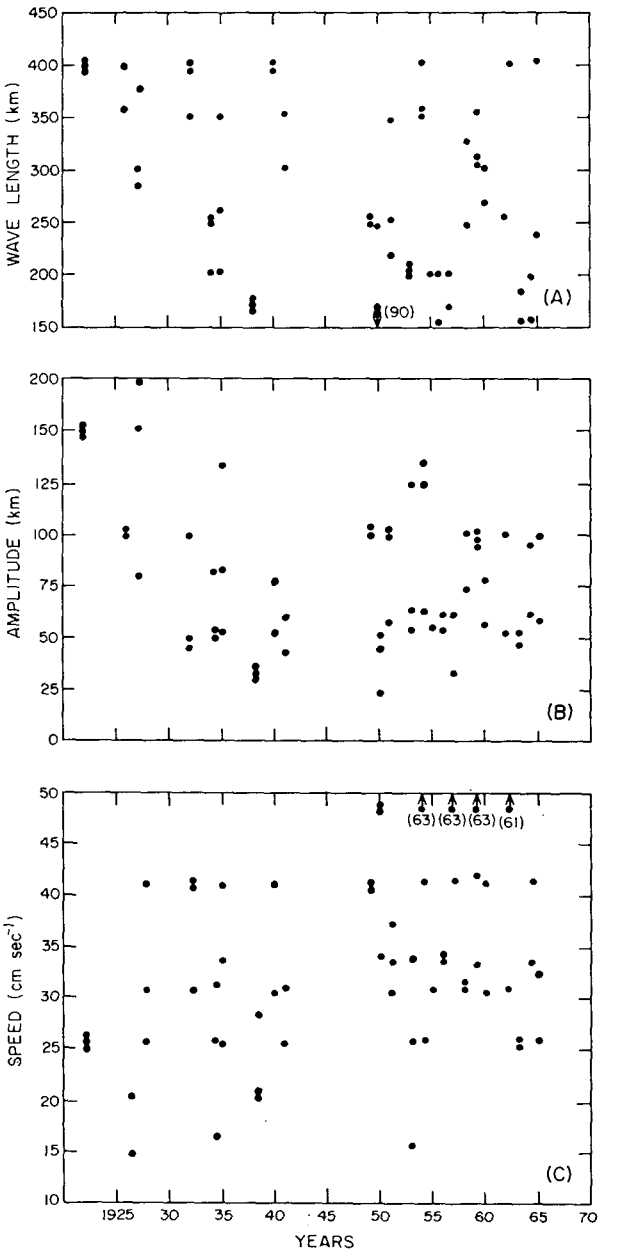

FIG. 15. Yearly distribution of meander parameters.

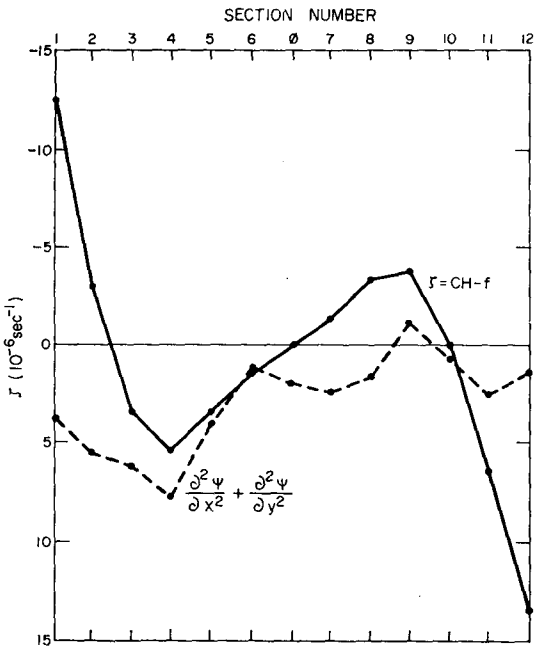

FIG. 16. Vertical component of vorticity along the meander defined by the 971.1 dm contour, mean April topography (see Fig. 2 for section location).

The results are compared in Fig. 16 (for section locations see Fig. 2). At section 1, the relative vorticity calculated from $\zeta = CH - f$ is negative because of the shallow depth over the Southeast Newfoundland Ridge. The current, setting southeasterly, then passes into deeper water and ζ becomes positive. As the current turns northward, it again moves into shallower water, attains negative vorticity, and then recurves eastward completing the meander.

The curve $\zeta = (\partial^2\psi/\partial x^2) + (\partial^2\psi/\partial y^2)$ has an initial positive value at section 1 because of the strong velocity shear across the Gulf Stream. Proceeding along the streamline, ζ becomes more positive, attaining a maximum at section 4 and then approaches zero near the wave node. The curves calculated by the two methods diverge between sections 6–8 (the same effect was also noted for the months of May and June), but then both achieve a relative minimum value at section 9. The correlation breaks down at section 12.

Considering the crudeness of the calculations, we feel the good agreement between the major features of the two curves argues for a rather strong bathymetric control of the meander pattern. At the northern end of the meander (section 12), one could infer that the baroclinicity decouples the actual surface flow from the bathymetry.

Acknowledgments. This study was supported by the Office of Naval Research under Contract N000 14-67-A-0103-0014.

APPENDIX A

International Ice Patrol Cruises U. S. Coast Guard, 1922–65

Year	Inclusive dates	Year	Inclusive dates
1922	11 April–5 May	1951	3–15 April
	3–30 May		23 May–4 June
	23 May–18 June	1952	4–16 June
1926	29 April–5 May	1953	3–14 April
	25–29 June		28 April–9 May
1927	6–10 April		6–17 June
	21–25 April	1954	1–15 April
	10–18 May		26 April–8 May
	29 May–3 June		27 May–11 June
	9–21 June	1955	1–15 April
1932	19 April–5 May	1956	1–13 April
	21–29 May		19 May–1 June
	13–19 June	1957	4–18 April
1934	19–26 April		1–12 May
	17–25 May	1958	3–15 April
	12–21 June		23 May–5 June
1935	10–20 April	1959	5–18 April
	8–18 May		30 April–11 May
	4–10 June		27 May–6 June
1938	31 March–11 April	1960	2–17 April
	27 April–7 May		18 June–1 July
	24 May–6 June	1962	1–13 April
	21 June–3 July		23 May–3 June
1940	30 March–9 April	1963	30 March–8 April
	23 April–3 May		14–25 May
	17–23 May	1964	15–27 March
	24–29 May		5–16 April
	12–18 June		2–13 May
1941	29 March–10 April		9–19 June
	15–18 April	1965	30 March–7 April
	10–20 May		19–25 May
1949	13–23 April		
	7–17 May		
1950	6–19 April		
	2–13 May		
	9–20 June		

APPENDIX B

Possible Biasing of Conclusions

During the 67 cruises listed in Appendix A, a total of 5627 IIP stations were taken, of which 3002 were within the grid spaces of Fig. 6. In order to examine whether conclusions about the geographical distribution of eddies might be biased by the distribution of data, Table 5 was prepared. If there were significant

TABLE 5. Distributions of eddies and IIP stations.

Grid no.	Number of cyclonic eddies	Percent of cyclonic eddies	Number of IIP stations	Percent of stations
1	3	13.6	160	5.3
2	5	22.7	530	17.7
3	2	9.1	256	8.5
4	1	4.5	66	2.2
5	0	0	428	14.3
6	8	36.4	601	20.0
7	0	0	400	13.3
8	3	13.6	561	18.7
Total	22	99.9	3002	100.0

bias, columns 3 and 5 should be correlated. However, the linear regression coefficient for these columns is only 0.52, so that the zero correlation hypothesis cannot be rejected at the 5% level. There is therefore no good reason to suspect biasing.

We note that a total of 19 seasons are missing from the listing in Appendix A. During 16 of these, there were either no cruises, no hydrographic casts, or the dynamic topographies were unavailable or inadequate for analysis. The dynamic charts from 1939, 1948 and 1961, based on 349 stations within the grid, were inadvertently omitted from the original analysis; a subsequent inspection, however, shows that their inclusion does not significantly affect any of the earlier results or conclusions.

REFERENCES

Barkley, R. A., 1968: The Kuroshio-Oyashio front as a compound vortex street. *J. Marine Res.*, **26**, 83–104.

Hansen, D. V., 1970: Gulf Stream meanders between Cape Hatteras and the Grand Banks. *Deep-Sea Res.*, **17**, 495–511.

Morgan, C. W., 1969: Oceanography of the Grand Banks region of Newfoundland in 1967. *U. S. Coast Guard Oceanogr. Rept.* No. 19, 209 pp.

Proudman, J., 1953: *Dynamical Oceanography*. New York, Wiley 409 pp.

U. S. Coast Guard, 1922–65: International Ice observation and ice patrol service in the North Atlantic Ocean (from 1960, called Report of the International Ice Patrol Service in the North Atlantic Ocean). *Bull.*, Nos. 10, 15, 16, 22, 24, 25, 28, 30, 31, 35–46, 48–51.

Warren, B. A., 1963: Topographic influences on the path of the Gulf Stream. *Tellus*, **15**, 167–183.